11. SLOWING DOWN SOLUTION

11.1 Method of Solution

Application of the method of characteristics to (9.19) yields the slowing-down distribution. For $v<v_o$, (9.19) can be rewritten as:

$$\frac{df}{dt} = \frac{\partial f}{\partial t} + \dot{v}\,\frac{\partial f}{\partial v} + \dot{\zeta}\,\frac{\partial f}{\partial \zeta} + \dot{\psi}_x\,\frac{\partial f}{\partial \psi_x} = \frac{f}{v^2}\,\frac{\partial \tilde{U}}{\partial v}\,, \tag{11.1}$$

where the slowing-down drift rates are found using (9.16)-(9.17):

$$\dot{v} = \frac{-\tilde{U}}{v^2} \tag{11.2}$$

$$\dot{\zeta} = \frac{G_x c\gamma B'_{ex}}{v^4\psi_x(B'_{ex}-B'_{ox})}\left(\frac{1-\zeta^2}{1+\zeta^2}\right)\widetilde{U(\psi_x-\psi)}\,, \tag{11.3}$$

$$\dot{\psi}_x = \frac{-2G_x c\gamma B_x}{v^4\psi_x(B'_{ex}-B'_{ox})}\left(\frac{\zeta}{1+\zeta^2}\right)\widetilde{U(\psi_x-\psi)}\,. \tag{11.4}$$

Integration of (11.1), using (11.2) to write, $dt = -v^2dv/\tilde{U}$, gives:

$$f = f\,(v_o,\zeta_o,\psi_{xo})\;\tilde{U}\,(v_o,\zeta_o,\psi_{xo})/\tilde{U}(v,\zeta,\psi_x), \tag{11.5}$$

which can be further simplified by substitution from (10.1):

$$f = \varepsilon(v_o,\zeta_o,\psi_{xo})/4\pi\tilde{U}(v,\zeta,\psi_x). \tag{11.6}$$

Note that (11.6) makes sense only when the coordinates (v,ζ,ψ_x) lie along the characteristic obtained by solving the system of ordinary differential equations (11.2)-(11.4) with the initial condition (v_o,ζ_o,ψ_{xo}).

11.1.1 The Invariant, μ/E

An important property of the slowing down distribution can be derived from this solution. By taking the ratio of (11.3) and (11.4) and integrating the resulting exact differential, the result is:

$$\mu/E = [1-\zeta^2(t)]/B_x(t) = \text{constant}. \tag{11.7}$$

Physically, this invariant arises because there is a negligible amount of pitch angle scattering during the slowing down. Alternately, the multiple time-scale discussion by Trubnikov [46] can be used to infer (11.7). This result can also be found by following Hazeltine's derivation [96] of the gyro-averaged derivative of μ, beginning with the Lorentz equations and including slowing-down losses. Meka [97, 121] previously obtained (11.7) for α's slowing in low-β tokamaks assuming the Knorr-form [23] for the magnetic field.

11.1.2 Slowing Down Drifts

The direction of the drifts in (11.3)-(11.4) is also important:

$$\text{sgn}(\dot{\zeta}) = \text{sgn}\left(\frac{B'_{ex}}{B'_{ex}-B'_{ox}}\right) = \begin{cases} +, & R_x > R_o \text{ and } B'_{ex} > 0 \\ -, & \text{otherwise} \end{cases} \tag{11.8a}$$

$$\text{sgn}(\dot{\psi}_x) = \text{sgn}\left(\frac{-\zeta}{B'_{ex}-B'_{ox}}\right) = \begin{cases} +, & R_x > R_o \text{ and } B'_{ex} > 0 \text{ and } \zeta < 0 \\ -, & \text{otherwise} \end{cases} \tag{11.8b}$$

As illustrated in Fig. 11.1, fast ions approach some "nominal" flux surface as they slow down to form small banana-width (thermalized) orbits. Since co-circulating and trapped orbits have ψ_x shifted outward in R, the corresponding ψ_x-drift is inward ($\dot{\psi}_x < 0$). Likewise, since counter-circulating orbits have ψ_x shifted inward in R, the ψ_x-drift is toward the magnetic axis ($\dot{\psi}_x < 0$). The positive ψ_x drift is a new (though small) finite-β effect occurring only for counter-going ions, where $R > R_o$ in the portion of the minimum-B well for which $B'_{ex} > 0$. The corresponding region of COM space is small, lying between $\zeta = 0$ and the right-hand o-type stagnation orbit boundary. The $\dot{\zeta}$-drift occurs to conserve μ/E in the presence of the $\dot{\psi}_x$-drift. These results are consistent with the inward drifts for co-going particles ($\dot{\psi}_x < 0$ for $\zeta > 0$) found by Cordey [45] and Killeen et al [77], but are in apparent contradiction with the outward drifts for counter-going ions found by Refs. 45 and 77. However, this discrepancy is due to an ambiguity in definitions for $\zeta = v_{\parallel}(\psi=\psi_x)/v$, used here, and $\xi = v_{\parallel}(\theta=0)/v$, used in Refs. 18, 45 and 77. The definition for $\xi > 0$ corresponds to ψ_x, which is consistent with the usage here, but $\xi < 0$ corresponds to evaluation at ψ_n for which the drift <u>is</u> outward (c.f. Fig. 11.1) and is consistent with Refs. 45 and 77. The results of Petrie and Miley [8] also show a net inward, slowing-down drift by using a model which apportions all the slowing contributions at the two points $\psi = \psi_x$ and $\psi = \psi_n$.

The magnitude of the drifts is an important result. In the limit $v_{ion} << v << v_e$, the parameter, U, in (9.19) becomes:

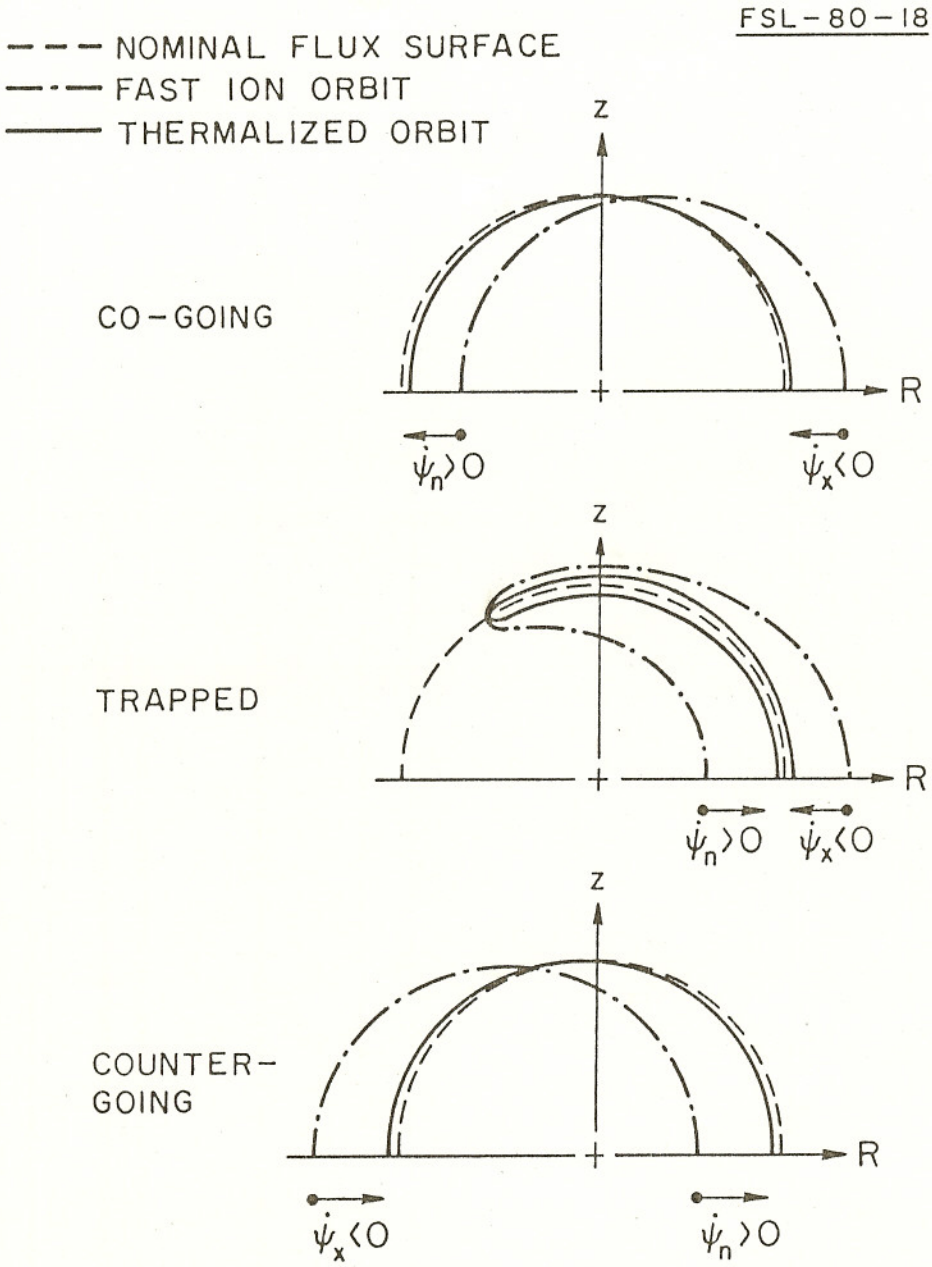

Figure 11.1 Representation of fast ion approaching some nominal flux surface during thermalization for (a) co-going, (b) trapped, and (c) counter-going ions.

$$U = (v_c^3 + v^3)/\tau_s, \tag{11.9}$$

$$v_c^3 = \frac{3\sqrt{\pi}}{4}\frac{m_e}{m_i} v_e^3 , \tag{11.10}$$

$$\tau_s = \frac{3\pi^{3/2}\varepsilon_o^2 m_e m v_e^3}{Z^2 e^4 n_e \ln \Lambda} . \tag{11.11}$$

As before, m_e and m_i are the electron and background ion masses; n_e is the electron particle density, and $v_e = \sqrt{2kT_e/m_e}$. Combining (11.9)-(11.11) with (11.2-11.4), and applying simple scaling arguments, one finds for typical ETF equilibria:

$$\frac{\dot{\psi}_x}{\psi_x - \psi_n} \sim \alpha_\psi \frac{\dot{v}}{v} , \text{ with } 0.25 < \alpha_\psi < 0.7, \tag{11.12}$$

$$\dot{\zeta} \sim \alpha_\zeta \frac{\dot{v}}{v_o} , \text{ with } 0 < |\alpha_\zeta| < 0.05. \tag{11.13}$$

Since $(\psi_x - \psi_n)$ is a measure of the poloidal gyroradius, (11.12) implies that the net slowing-down drift in ψ_x is ~ 1/2 of a banana width in slowing from velocity, v, to thermal. This is consistent with the arguments of the previous paragraph. The ζ-drift, while small, is sufficient to eliminate any net thermal α-current. Numerical calculations show that (11.12)-(11.13) are valid from 3.5 MeV to thermal energies. Since the poloidal gyroradius is proportional to velocity, we find

$$\psi_{xo} - \psi_x(t) \sim \alpha_\psi(\psi_x-\psi_n)_o(1-v/v_o), \tag{11.14}$$

where $(\psi_x-\psi_n)_o$ indicates $(\psi_x-\psi_n)$ at $v = v_o$, and similarly that:

$$\zeta(t) - \zeta_o \sim \alpha_\zeta(1-v/v_o). \tag{11.15}$$

Thus, the coefficients α_ψ and α_ζ characterize not only the drift rates but the total drifts in slowing to thermal speeds. These results apply to both of the equilibria listed in Table 10.1.

11.1.3 Method of Characteristics Solution

With the above properties in hand, the system (11.2)-(11.4) can be reduced to the solution of a single differential equation. Since the flux-surface-averaged quantities (c.f. eqns. 11.21-11.25) require a knowledge of the distribution function over (v,ζ,ψ_x) space, it is unnecessary to know the explicit time dependence. (Even for non-steady-state problems, not of interest here, the explicit time dependence of $f(v,\zeta,\psi_x,t)$ must be found only if the time-scale for evolution of the equilibrium is $\leq \tau_s$.) We therefore choose the speed, v, as the independent variable; this choice permits the differential equations to be rewritten as:

$$\frac{d\zeta}{dv} = \frac{\dot{\zeta}}{\dot{v}} = \frac{-G_x c\gamma B'_{ex}}{v^2\psi_x(B'_{ex}-B'_{ox})}\left(\frac{1-\zeta^2}{1+\zeta^2}\right)\frac{\widetilde{U(\psi_x-\psi)}}{\tilde{U}}, \tag{11.16}$$

$$\frac{d\psi_x}{dv} = \frac{\dot{\psi}_x}{\dot{v}} = \frac{2G_x c\gamma B_x}{v^2\psi_x(B'_{ex}-B'_{ox})}\left(\frac{\zeta}{1+\zeta^2}\right)\frac{\widetilde{U(\psi_x-\psi)}}{\tilde{U}} \tag{11.17}$$

In addition, (11.7) can be used to eliminate (11.16):

$$\zeta = \pm \sqrt{1 - \frac{B_x}{B_{xo}} (1-\zeta_o^2)} \quad , \tag{11.18}$$

in which the sign ambiguity is resolved from:

$$\mathrm{sgn}(\zeta^{i+1}) = \begin{cases} +, \ R_x > R_o \text{ and } \zeta^{(i)} > 0, \\ +, \ R_x > R_o, \zeta^{(i)} < 0, \text{ and } |\zeta^{(i+1)}| > |\zeta^{(i)}|, \\ -, \ R_x < R_o, \end{cases}$$

where $\zeta^{(i)}$ corresponds to $v^{(i)}$ and $\zeta^{(i+1)}$ to $v^{(i)} + \Delta v$ in the numerical integration. When $R_x > R_o$, $\zeta^{(i)} < 0$, and $|\zeta^{(i+1)}| \leq |\zeta^{(i)}|$, the sign ambiguity is resolved by numerically integrating (11.16); this is a very small class of cases, corresponding to orbits having $\dot{\psi}_x > 0$ (discussed above). The solution to (11.17)-(11.18) is of the form:

$$\psi_x = \psi_x(v_i; v_o, \zeta_o, \psi_{xo}), \text{ and} \tag{11.19}$$

$$\zeta = \zeta(v_i; v_o, \zeta_o, \psi_{xo}). \tag{11.20}$$

Solving (11.16)-(11.17) completely describes the slowing-down problem, including the large banana width effects and slowing-down drifts in realistic non-circular, high-β equilibria.

11.1.4 Calculation of Integrals

To numerically evaluate the flux-surface averages, it is easiest to find $f(v_i,\zeta_j,\psi_{xk})$ on a specified rectilinear mesh, where $v_i = i\Delta v$, $\zeta_j = j\Delta\zeta$, $\psi_{xk} = k\Delta\psi_x$ for integral values of (i,j,k). This is done by taking (v_i,ζ_j,ψ_{xk}) as the starting point and integrating (11.17) backward in time to $v = v_o$, with corresponding values $\zeta(v_o) = \zeta_o$ and $\psi_x(v_o) = \psi_{xo}$. Using the source rate, $\tilde{s}(v_o,\zeta_o,\psi_{xo})$, found in Chapter 10, the distribution-function is obtained from (11.6). At each step in the v-integration, it is necessary to check that $\psi_x \leq \psi_{edge}$; if $\psi_x > \psi_{edge}$, then the starting point lies in a region of zero distribution function. That is, the inward slowing-down drifts carry the fast ions about half of a banana width inside the plasma edge, leaving no fast ions at the edge. The important flux-surface-averaged quantities are as follows: the alpha particle density profile,

$$\langle n_\alpha \rangle = \int f_\alpha d^3x d^3v \Big/ \int_{\psi_1}^{\psi_2} d^3x, \tag{11.21}$$

the alpha-particle current density profile,

$$\langle J_\parallel \rangle = \int ev\eta f_\alpha d^2x d^3v \Big/ \int_{\psi_1}^{\psi_2} d^2x, \tag{11.22}$$

the profile of alpha heating power per ion,

$$\langle P_e \rangle = \int f_\alpha m v \dot{v}_e d^3x d^3v \Big/ \int_{\psi_1}^{\psi_2} n_e d^3x, \tag{11.23}$$

$$<P_i> = \int f_\alpha m v \dot{v}_i d^3x d^3v \Big/ \int_{\psi_1}^{\psi_2} n_i d^3x, \tag{11.24}$$

and the net alpha particle current,

$$<I_\parallel> = \int e v \eta f_\alpha d^2x d^3v, \tag{11.25}$$

where $\dot{v}_i = \widetilde{v^3/\tau_s}$, and $\dot{v}_e = \widetilde{v_c^3/\tau_s}$, are the deceleration rates due to ions and electrons, respectively. These integrals are evaluated in the same way as the source rate integrals in Chapter 10, c.f. (10.16)-(10.17).

11.1.5 Boundary Conditions

The boundary conditions, at the o-type and x-type stagnation boundaries, are the only remaining aspect of this problem. Considering first the o-type stagnation boundary (lines A-B and F-G in Fig. 8.1c), the corresponding surface in (v,ζ,ψ_x) space can be written using (8.4):

$$W = B'_{ex} - B'_{ox}(v,\zeta,\psi_x) = 0 \tag{11.26}$$

where B'_{ox} is given by the RHS of (8.4). The normal to this surface is ∇W, while the tangent to a slowing-down characteristic is obtained from (11.2)-(11.4):

$$\frac{d\vec{v}}{dt} = \dot{v}\hat{v} + \dot{\zeta}\hat{\zeta} + \dot{\psi}_x\hat{\psi}_x. \tag{11.27}$$

Evaluating the dot product, $\nabla W \cdot d\vec{v}/dt$, using (11.26), and the condition that $B_{ox} = B_{on}$ for an o-type stagnation orbit, gives

$$\nabla W \cdot d\vec{v}/dt = \frac{\partial W}{\partial v}\dot{v} + \frac{\partial W}{\partial \zeta}\dot{\zeta} + \frac{\partial W}{\partial \psi_x}\dot{\psi}_x = 0. \tag{11.28}$$

This condition implies that characteristics in the vicinity of the o-type stagnation boundary (surface) move parallel to the boundary, i.e. have no component perpendicular to it. Consequently, no conservation condition is needed at this boundary. Looking next at the counter-going x-type boundary (line BCD in Fig. 8.1c), one sees from (11.8) that slowing drifts take particles away from this boundary because ζ decreases monotonically. Thus, conservation conditions are not needed at counter-going x-type stagnation boundary. Finally, at the (x-type) pinch boundary (line HI in Fig. 8.1c), the ζ-drifts (c.f. eqn. 11.8) carry the characteristics in the direction of decreasing ζ (arrows labelled 3 in Fig. 8.2b). Since adjacent segments across the pinch boundary are contiguous, velocity-space fluxes are trivially conserved. Here, as is typically the case in method-of characteristics solutions, the boundary conditions are implicitly included in the solution.

11.2 Results

The alpha particle profiles (c.f. eqns. 11.21-11.25) have been evaluated for three models. First, for comparative purposes, in-situ deposition is used to determine the electron and ion heating rate profiles:

$$(P_e)_{IS} = E_o \int_{\psi_1}^{\psi_2} G_e n_i n_2 \langle\sigma v\rangle_{12} d^3x \Big/ \int_{\psi_1}^{\psi_2} n_e d^3x, \tag{11.29}$$

$$(P_i)_{IS} = E_o \int G_i n_i n_2 \langle\sigma v\rangle_{12} d^3x \Big/ \int_{\psi_1}^{\psi_2} n_i d^3x. \tag{11.30}$$

Here, $G_e = 1-G_i$, and G_i is the fraction of power into ions found by Stix [54]:

$$G_i = \left(\frac{v_c}{v_o}\right)^2 \int_0^{(v_o/v_c)^2} \frac{dx}{1+x^{3/2}} . \tag{11.31}$$

For $v_o/v_c > 1$, (11.31) can be conveniently expanded in a Taylor series and integrated to yield:

$$G_i = \left(\frac{v_c}{v_o}\right)\left(1 - \frac{1}{4y} + \frac{1}{7y^2} - \frac{1}{10y^3} + \frac{1}{13y^4} - \ldots\right) , \tag{11.32}$$

where $y = (v_o/v_c)^3$. For $v_o/v_c > 2$, (11.32) converges well; for $v_o/v_c < 2$, (11.31) is evaluated numerically. In the second model, the ζ- and ψ_x-drifts are set to zero, to demonstrate the size of their effect on the profiles. The distribution function in this approximation is:

$$f(v,\zeta,\psi_x) = s(v_o,\zeta_o,\psi_{xo})/4\pi\tilde{U}(v,\zeta_o,\psi_{xo}) . \tag{11.33}$$

Finally, the large-banana-width slowing-down distribution, including ζ- and ψ_x-drifts is obtained by integrating (11.17) via a second-order Runga-Kutta method.

The results of these three models for various equilibria (c.f. Table 10.1) are shown in Figs. 11.2-11.3. The prominent peakedness of the in-situ heating curves is strongly weighted by the alpha source function, $\dot{n}_\alpha = n_1 n_2 \langle\sigma v\rangle_{12}$, as the alphas slow down at their birth positions. Large banana-width orbits smear the heating deposition over large regions of the plasma (c.f. Fig. 10.2). This finite-banana spreading causes the flux-surface-averaged profiles without drifts ($\dot{\psi}_x=0$, $\dot{\zeta}=0$) to be less centrally peaked, but substantially above the in-situ curve at the edge ($\psi/\psi > 0.6$). The flux-surface-averaged profiles including drifts ($\dot{\psi}_x\neq 0$, $\dot{\zeta}\neq 0$) lie below the second case since the inward ψ_x-drift causes slightly more core heating while depleting the edge.

The net positive alpha current (in the direction of the plasma current) is due to finite banana-width effects (see Figs. 11.2-11.3). From the values of $\langle I_\parallel \rangle$ shown in Table 10.1, we find an improved estimate for the alpha current is:

$$I_\parallel \sim .3\langle \dot{I}_\parallel \rangle \tau_s \,. \tag{11.34}$$

The current contributions due to co- and counter-going orbits tend to cancel, leaving mainly the trapped contribution (consistent with Cordey's result [45]). For large banana-width trapped orbits, the path length along the co-going part is longer than the counter-going

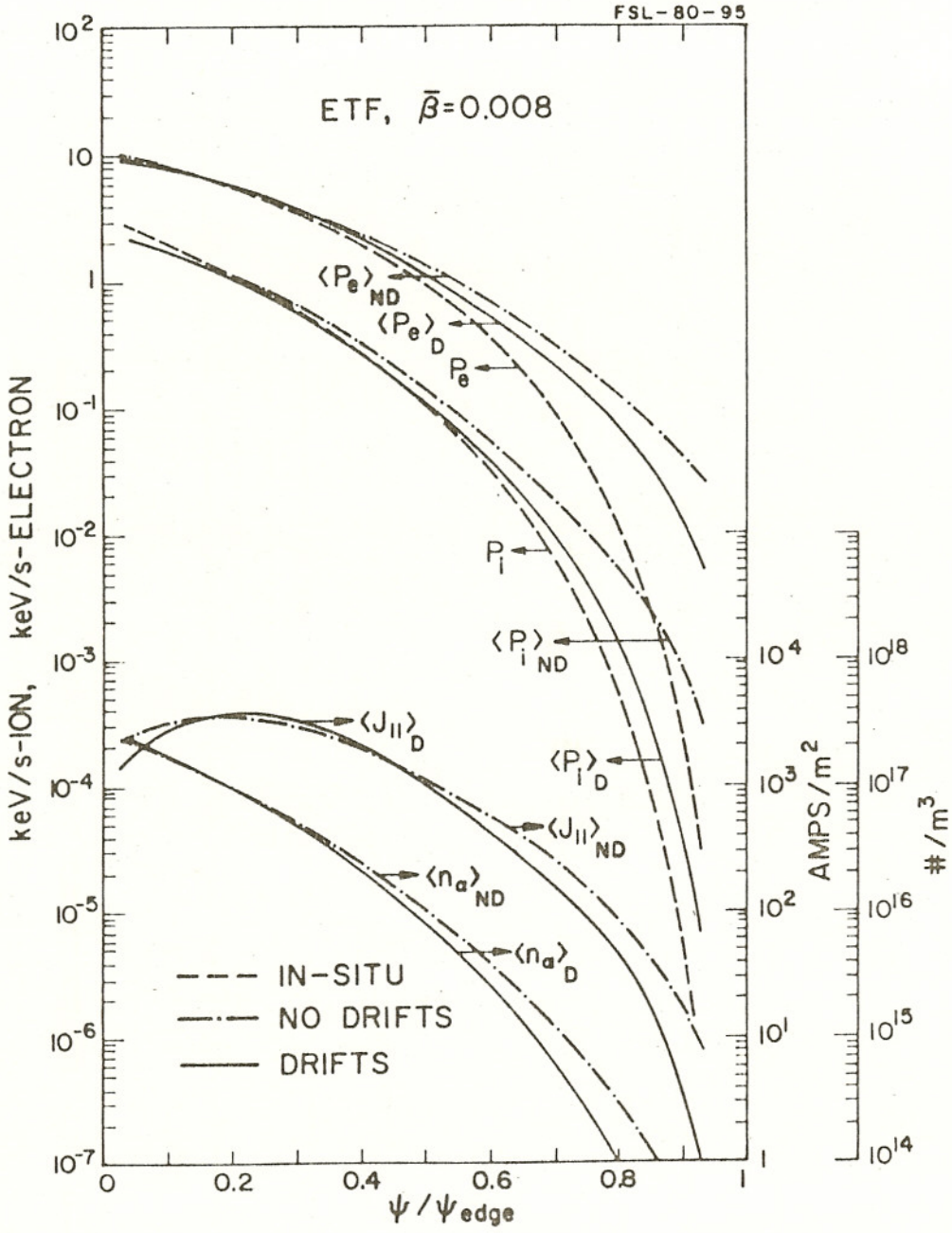

Figure 11.2. Alpha particle density, current and heating profiles in a D-shaped ETF ($\bar{\beta}$ = 0.008) reactor. In-situ deposition is indicated by $P_{e,i}$; flux-surface-averaged profiles, without the ψ_x and ζ-drifts, are labelled with the subscript "ND," with the ψ_x and ζ-drifts, the subscript "D" is used.

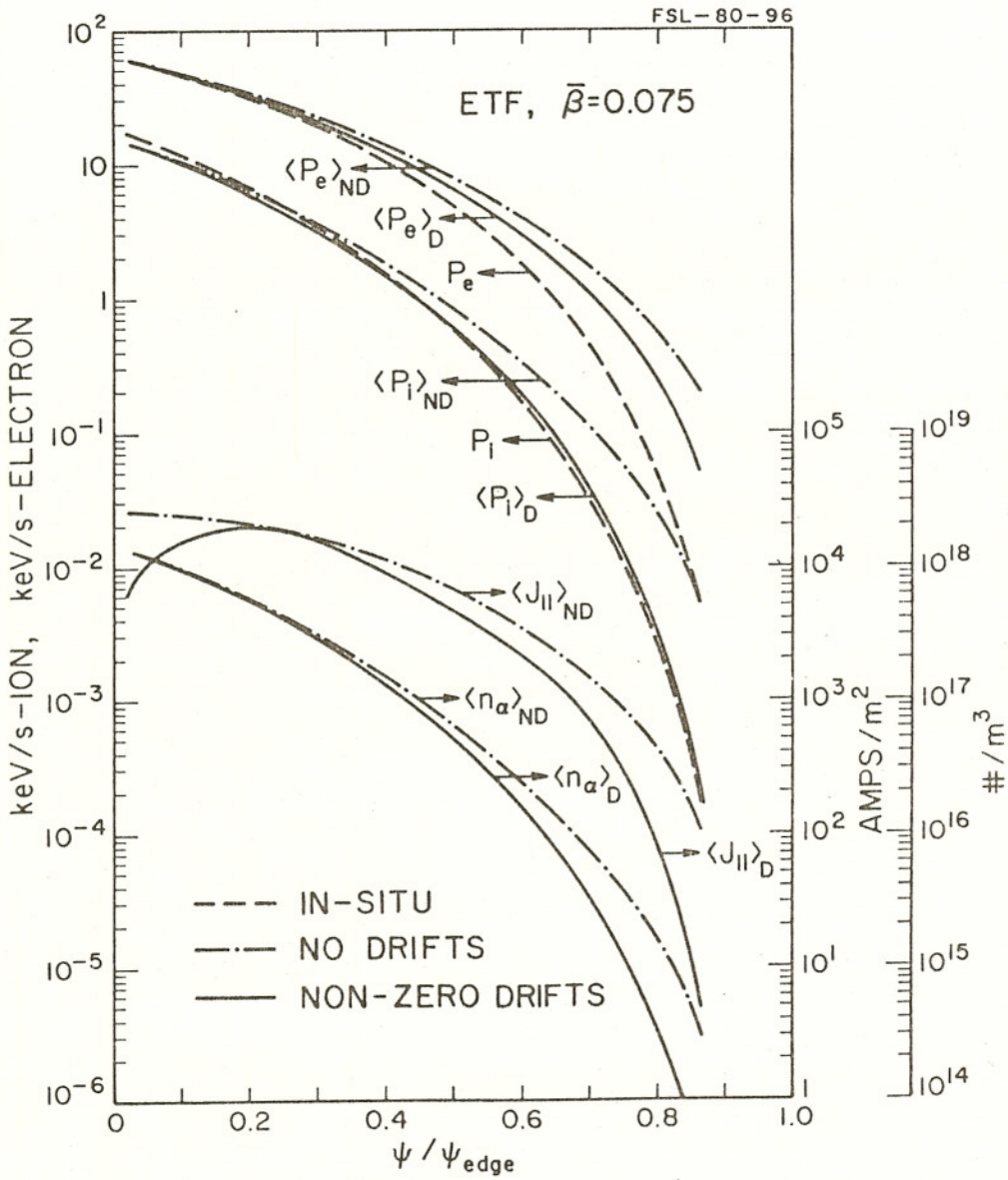

Figure 11.3. Alpha particle density, current and heating profiles in a D-shaped ETF ($\bar{\beta}$ = 0.075) reactor. In-situ deposition is indicated by $P_{e,i}$; flux-surface-averaged profiles, without the ψ_X and ζ-drifts, are labelled with the subscript "ND," with the ψ_X and ζ-drifts, the subscript "D" is used.

part. This results in a net co-current, since crudely speaking, the travel time goes like (connection length)/v. More realistically, most trapped particles have a net co-current (as described above), while a few trapped ions have a net counter-current. The x-stagnation orbits are an example of the latter because the bounce time contribution becomes infinite at the pinch point, where the motion is counter-going. From eqn. E.13 (see Appendix E), the resulting current is then $I_s \propto N_s Zev\eta_p < 0$, where N_s is the number of particles on the x-stagnation orbit and η_p is the cosine of the pitch angle at the pinch point. However, the bounce time is very long compared to the coulomb scattering time, implying that most ions are scattered off x-stagnation orbits. Summing these co- and counter-current contributions over all of phase space (c.f. eqn. 11.25) yields a net co-going current. As expected, the additional effects of the negative ζ-drift decreases the alpha current, in comparison to the no-drift case. The inward ψ_x-drift depletes the current density at the edge, while making the inner $\langle J_\parallel \rangle$ profile more peaked.

The background plasma response is not included in the calculation of the alpha particle current. Ohkawa [119] first suggested that fast ion injection in the co-going direction could form a toroidal plasma current. More recently, Hirshman [91] used a variational technique to find the Green's function for the plasma current response to fast ions, while Cordey et al. [92] obtained the induced plasma current via a perturbation method. The additional effect of

trapped electrons in the banana regime has been evaluated by Start et al. [93]. The net fast-ion-driven current in a circular cross-section tokamak is [114]:

$$I_{driven} = I_{fast}\left[1 - \frac{Z}{Z_{eff}} + \frac{1.46\ Z}{Z_{eff}}\left(\frac{r}{R}\right)^{\frac{1}{2}} A\left(Z_{eff}\right) - \frac{1.2}{Z_{eff}}\left(\frac{v}{v_e}\right)^2\right], \quad (11.35)$$

where $A(Z_{eff}) \approx 1 + 0.7/Z_{eff}$[60], Z is the fast ion charge, and v_e is the electron thermal speed. The first term on the RHS of (11.35) is the α-current, $\langle I_{\parallel} \rangle$, calculated above. The second term is the "shielding current" due to streaming of electrons, caused by collisional momentum transfer from the fast ions. The third term describes the effect of banana-trapped electrons. The last term accounts for electron-electron collisions, for the fact that the electron distribution cannot be represented by a displaced-Maxwellian, and for the velocity dependence of the friction force between the electrons and fast ions. The α-driven current, in turn, can serve as a seed current for the bootstrap effect [94]. Considering practical heating rates and seed current values, the total current, I_{tot}, might become approximately 10 times the seed current, I_{driven}[95]. This is significant since the α-current might then drive part of the steady-state plasma current, reducing the volt-sec requirements for a reactor [90], though not affecting the volt-sec requirements for start-up.

Stacey and Sigmar [117] have determined the full response of a non-circular axisymmetric tokamak plasma to particle and momentum sources. They find that a net toroidal momentum input produces an

additional contribution to the toroidal current density, beyond those discussed above. One such source would be the α-driven, bootstrap-enhanced current, I_{tot}. Alpha particle losses to the tokamak first wall are another current input [16] (due to a net loss of momentum). However, such losses are unimportant (< 1% contribution) in the large plasmas of interest here. A proper evaluation of these effects including the non-circular cross section is beyond the scope of this work.